Research Square

Preprints are preliminary reports that have not undergone peer review.
They should not be considered conclusive, used to inform clinical practice,
or referenced by the media as validated information.

Influence of bioactive glass particle size in resin-based fissure sealants on the remineralization of adjacent enamel: an in vitro study

Gözde Asena Bayraktar Acar
Çekmeköy Oral and Dental Health Center
Ali Can Özarslan
Istanbul University-Cerrahpaşa Faculty of Engineering
Ceren Emir
Yıldız Technical University
Sevil Yücel
Yıldız Technical University
Pınar Kınay Taran
ptaran@bezmialem.edu.tr

Bezmiâlem Vakıf Üniversitesi

Research Article

Keywords: Bioactive glass, dental caries, fissure sealant, remineralization, nanoindentation, nano-sized particles

Posted Date: November 6th, 2026

DOI: https://doi.org/10.21203/rs.3.rs-11348278/v1

License: This work is licensed under a Creative Commons Attribution 4.0 International License.
Read Full License

Additional Declarations: No competing interests reported.

Abstract

Background

Bioactive glass (BAG)-modified fissure sealants may promote enamel remineralization, but the influence of BAG particle size remains unclear. This study aimed to compare the effects of micro-sized, nano-sized, and hybrid BAG particles incorporated into a resin-based fissure sealant on the remineralization of adjacent enamel using nanoindentation and SEM–EDS.

Methods

Forty-five sound human enamel specimens were randomly assigned to five groups (n = 9): unsealed negative control, conventional sealant, micro-BAG (15 wt%), nano-BAG (15 wt%), and hybrid BAG (7.5 wt% micro + 7.5 wt% nano). All specimens underwent artificial demineralization before the sealants were applied. Enamel adjacent to the sealant was assessed by nanoindentation (nanohardness, elastic modulus) before and after a 7-day pH-cycling regimen, and surface hardness recovery (%SHR) was calculated. Scanning electron microscopy with energy-dispersive X-ray spectroscopy (SEM–EDS) was performed descriptively on one specimen per group. Data were analyzed using paired t tests (within groups) and one-way ANOVA with Duncan's post hoc test (between groups) (α = 0.05).

Results

Mean nanohardness increased in all groups after pH cycling, but the increase was statistically significant only in the nano-BAG group ($P = 0.036$). Nanohardness differed among groups after demineralization ($P = 0.044$) and after pH cycling ($P = 0.031$), with the unsealed negative control showing the highest values at both stages. No significant differences were found among groups in elastic modulus ($P = 0.106$ and 0.056) or %SHR ($P = 0.820$). SEM–EDS showed higher calcium content and Ca/P ratios in BAG-containing groups, with the highest values in the nano-BAG group; no statistical comparison was performed.

Conclusions

Within the limitations of this in vitro study, only the nano-BAG group showed a significant increase in enamel nanohardness after pH cycling, with no significant differences among the sealant groups. These preliminary findings support further investigation of nano-BAG–modified sealants, including larger samples, characterized fillers, and mechanical and ion-release testing.

BACKGROUND

Dental caries remains a prevalent global public health challenge in childhood, imposing significant socio-economic burdens and reducing quality of life [1, 2]. To minimize treatment costs and preserve tooth structure, preventive and non-invasive approaches are prioritized to arrest or reverse early-stage lesions [1, 2]. Despite the declining incidence of smooth surface caries, partly due to these practices, occlusal surfaces remain highly susceptible to decay. This persistence is attributed to the complex morphology of pits and fissures, which facilitates the mechanical retention of biofilm and nutrients [3, 4].

Pit and fissure sealants are widely utilized and effective clinical interventions for preventing occlusal caries by establishing a physical barrier between the tooth morphology and the oral environment [5]. Due to their favorable mechanical properties and retention, light-curing resin-based sealants remain the primary choice in clinical practice [6]. However, these materials are susceptible to polymerization shrinkage, which may lead to microleakage and increased plaque adhesion. Consequently, partial material loss or microleakage may facilitate the development of secondary caries, which can compromise sealant success [7]. To counteract these limitations while retaining their advantageous properties, resin-based sealants are increasingly modified with various antibacterial or remineralizing agents [7–9].

Fluoride has long been incorporated into resin-based fissure sealants to leverage its remineralizing and antibacterial properties. While some studies support its efficacy [10–12], clinical findings are often contradictory, with several reports showing no significant difference in caries incidence between fluoridated and non-fluoridated sealants [13, 14]. A key limitation is the inferior fluoride-recharge capacity and lower ion release of fluoride-releasing resin sealants compared to glass ionomer cements (GICs) [15, 16]. Thus, the clinical superiority of these materials remains unproven [17]. To address these shortcomings, research has shifted toward alternative agents such as CPP-ACP, chlorhexidine, and quaternary ammonium compounds to enhance both antibacterial and remineralizing activities [9, 18].

Originally developed by Hench et al. in 1969, bioactive glass (BAG) is a biocompatible material characterized by its ability to form a hydroxyapatite-like layer upon contact with physiological fluids [19]. The composition of BAG can be precisely tailored to achieve specific clinical outcomes, such as enhancing antibacterial efficacy through the addition of elements like silver. Beyond compositional modifications, particle size may also influence bioactivity; in particular, reducing BAG particles from the micrometric to the nanometric scale increases the reactive surface area, which may accelerate ion release and enhance remineralization potential [20, 21]. A combination of micro- and nano-sized particles could, in principle, provide both early and sustained ion release. While BAG-modified fissure sealants have shown promise in neutralizing acids and inhibiting demineralization, comparative evidence on how nano-sized versus micro-sized BAG particles influence their remineralizing effect on adjacent enamel remains limited [7, 8, 22]. Therefore, this study aimed to compare the effects of fissure sealants incorporating micro-sized, nano-sized, and hybrid BAG particles on the remineralization of enamel adjacent to the sealant, using nanoindentation and SEM–EDS. The null hypothesis was that BAG particle size would not affect the remineralization of enamel adjacent to resin-based fissure sealants.

METHODS

The experimental design of the study is summarized in Fig. 1.

Synthesis of micro- and nano-sized bioactive glasses

Micro-sized 45S5 BAG (BONE-G Active Ref: Bga025.05/2, Meta Biomühendislik ve Arge Hizmetleri A.Ş., Istanbul, Turkey), composed of 24.5 wt% Na_2O, 24.5 wt% CaO, 6 wt% P_2O_5, and 45 wt% SiO_2, was obtained by the melt-derived method. Production of melt-derived 45S5 BAG was detailed in previous studies [23]. To obtain a powder with particle sizes below 100 μm, the glass was processed using a planetary ball mill (PM 400; RETSCH GmbH, Haan, Germany).

Nano-sized BAG (Department of Bioengineering, Faculty of Chemistry and Metallurgy, Yıldız Technical University, Istanbul, Turkey), composed of 24.4 wt% Na_2O, 26.9 wt% CaO, 2.6 wt% P_2O_5, and 46.1 wt% SiO_2, was obtained by the sol-gel method. Production of sol-gel BAG was detailed in previous studies [24]. The nano-sized particles had a diameter of 90–110 nm.

Preparation of experimental resin-based fissure sealants

Experimental fissure sealants were prepared by incorporating 15 wt% of micro- or nano-sized BAG fillers into a commercial resin-based fissure sealant (Helioseal F Plus; Ivoclar Vivadent AG, Schaan, Liechtenstein). For the hybrid sealant, 7.5 wt% micro-sized and 7.5 wt% nano-sized BAG particles (total 15 wt%) were incorporated. To prevent premature polymerization, all BAG particles were integrated into the resin matrix via manual homogenization using a metal spatula under darkroom conditions. Manual mixing was carried out until a visually uniform dispersion was achieved. The resulting experimental sealants were immediately transferred into light-shielded containers and stored until use.

Preparation of tooth specimens

The sample size was calculated using G*Power software (version 3.1.9.7; Heinrich Heine University, Düsseldorf, Germany) for a repeated-measures ANOVA (between factors; five groups, two measurements). Assuming an α of 0.05, a power (1 − β) of 0.80, a large effect size (f = 0.50), and a correlation of 0.5 among repeated measures, a minimum of 41 specimens (approximately 8 per group) was required. To allow for this, nine specimens per group (total n = 45) were included. The study protocol was approved by the Institutional Review Board of … (Approval No: 2021/128), and written informed consent was obtained from all patients prior to tooth collection. Accordingly, 45 caries-free, extracted human third molars were utilized. Following soft tissue debridement, the teeth were stored in distilled water at 4°C. The roots were sectioned at the cementoenamel junction, and the crowns were vertically embedded in epoxy resin with the occlusal surfaces exposed. To obtain a flat, smooth substrate suitable for nanoindentation analysis, the enamel surfaces were sequentially polished using 600-, 1200-, and

2400-grit silicon carbide abrasive papers under continuous water cooling. Finally, the prepared specimens were randomly allocated into five experimental groups (n = 9 per group):

- Group 1 (Negative control): Unsealed demineralized enamel,
- Group 2 (Control): Sealed with conventional resin sealant (Helioseal F Plus),
- Group 3 (Micro-BAG): Sealed with 15 wt% micro-sized BAG-incorporated sealant,
- Group 4 (Nano-BAG): Sealed with 15 wt% nano-sized BAG-incorporated sealant, and
- Group 5 (Hybrid-BAG): Sealed with hybrid BAG-incorporated sealant (7.5 wt% micro + 7.5 wt% nano).

Caries induction, sealant application, and pH cycling

To induce artificial caries-like lesions, each specimen was immersed in a demineralization solution (2.2 mmol/L $CaCl_2$, 2.2 mmol/L KH_2PO_4, 0.05 M acetic acid, 0.2 ppm F; pH adjusted to 5.0 with 1 M KOH) for 32 hours [25].

Following demineralization, Group 1 received no sealant application and served as the negative control. For Groups 2–5, the enamel surfaces were first etched with 37% phosphoric acid (Jade, Dharma Research, Inc., USA) for 15 s, rinsed with water for 15 s, and air-dried. Then, the respective commercial or experimental fissure sealants were applied to the etched enamel surfaces according to the manufacturers' instructions and polymerized for 20 seconds using a LED curing unit (VALO Cordless; 385–515 nm, 3200 mW/cm², Ultradent, South Jordan, UT, USA).

A 7-day pH-cycling protocol was applied to all specimens. The cycle consisted of 6 h of demineralization followed by 18 h of remineralization. The content of the demineralizing solution was 1.5 mM $CaCl_2$, 0.9 mM KH_2PO_4, and 50 mM acetic acid, pH 5.0 whereas the remineralizing solution consisted of 1.5 mM $CaCl_2$, 0.9 mM KH_2PO_4, 130 mM KCl, and 100 mM Tris, pH 7.0. The solutions were prepared according to a modified version of the pH-cycling model described by Featherstone et al. [26] and were renewed daily. Specimens were rinsed with distilled water for 5 s and dried between immersions. After the cycle, specimens were rinsed and stored in distilled water until further analysis.

Nanoindentation analysis

The nanohardness (H_i) and elastic modulus (E_i) of the enamel were measured using a nanoindentation tester (Micro-Combi Tester, CSM Instruments, Switzerland) equipped with a Berkovich diamond indenter. Measurements were performed at two stages: after demineralization (before sealant application) and after the pH-cycling protocol. Because the sealant sites were predetermined, indentations were made on the enamel adjacent to the planned sealant margin, at a standardized distance of 50 μm from the planned sealant–enamel interface, which was marked with a reference line before sealant application. The same points were measured at both stages, including in the negative control group, which received no sealant. A maximum load of 100 mN was applied with a loading/unloading rate of 3.33 mN/s and a

dwell time of 10 s at maximum load. Hardness and elastic modulus were calculated from the load–displacement curves using the instrument software. Three indentations were made per specimen, and their mean value was used for analysis.

The percentage of surface hardness recovery (%SHR) was calculated using a modification of the formula described by Amaechi et al. [27]:

$$\%SHR = 100 \times \frac{H_{REM} - H_{DEM}}{H_{DEM}}$$

where H_{DEM} and H_{REM} are the nanohardness values after demineralization and after pH cycling, respectively.

Scanning Electron Microscopy with Energy-Dispersive X-ray Spectroscopy (SEM-EDS) Analysis

SEM–EDS analysis was performed as a descriptive, semi-quantitative assessment of the elemental composition of the enamel adjacent to the fissure sealant. Due to the exploratory nature of this analysis, one randomly selected specimen per group was evaluated after pH cycling. Each selected specimen was sectioned mesiodistally using a double-sided diamond wafering blade (0.5 mm, Isomet, Buehler, USA) under water cooling in a precision cutting machine (Mecatome T201 Press, France). The resulting sections were examined by SEM–EDS (EVO LS10, Zeiss, Oberkochen, Germany) to determine the elemental composition of the enamel. Prior to examination, the specimens were sputter-coated with gold (108 Auto Sputter Coater, Cressington Scientific Instruments, Watford, UK). Five measurement points were selected on the enamel adjacent to the fissure sealant base and analyzed at 10 keV. SEM images of the sealant–enamel interface were acquired at 1,000× (2,500× for the unsealed negative control) and are shown in Fig. 2. The atomic (at%) and weight (wt%) percentages of Ca, P, F, O, Na, and Si were calculated for each measurement point, and the Ca/P ratio was calculated from the weight percentages. Mean ± SD values were calculated from the five points of each specimen.

Statistical analysis

Statistical analysis was performed using SPSS software (version 23.0; IBM Corp., Armonk, NY, USA). The specimen was the unit of analysis (mean of three indentations). Normality was assessed using the Shapiro–Wilk test and homogeneity of variances using Levene's test. Within-group comparisons between the post-demineralization and post-pH cycling stages were performed using the paired-samples t test. Between-group comparisons were performed using one-way ANOVA followed by Duncan's multiple range test. SEM–EDS data were analyzed descriptively, without inferential statistics. The significance level was set at α = 0.05 (two-sided).

RESULTS

All 45 specimens (n = 9 per group) were included in the analysis. The nanohardness values of enamel specimens for each group measured after artificial demineralization and following the pH cycling regimen are presented in Table 1. One-way ANOVA revealed statistically significant differences among the groups both after demineralization (F = 2.706, P = 0.044) and after pH cycling (F = 2.970, P = 0.031). Because sealants had not yet been applied after demineralization, the differences at this stage represent baseline differences among groups. According to Duncan's test, the Negative control group showed the highest nanohardness at this stage (1.341 ± 0.545 GPa), which was significantly higher than that of the Control group (0.763 ± 0.311 GPa; P < 0.05), and the same pattern was observed after pH cycling (1.362 ± 0.402 vs. 0.854 ± 0.364 GPa). The Micro-BAG, Nano-BAG, and Hybrid-BAG groups did not differ significantly from either group at either stage. Mean nanohardness increased in all groups after pH cycling, but the increase was statistically significant only in the Nano-BAG group, rising from 1.044 ± 0.436 GPa to 1.159 ± 0.408 GPa (t(8) = − 2.511, P = 0.036). In contrast, no statistically significant within-group differences were detected in the Control (P = 0.373), Micro-BAG (P = 0.295), Hybrid-BAG (P = 0.082), or Negative control (P = 0.777) groups following pH cycling.

Table 1
Nanohardness values of enamel (Hi) in each group after demineralization and pH cycle

Group	**H_i after demineralization (GPa), mean ± SD**	**H_i after pH cycle (GPa), mean ± SD**	**Test statistic†**	***P*†**
Negative control	1.341 ± 0.545[b]	1.362 ± 0.402[b]	−0.293	0.777
Control	0.763 ± 0.311[a]	0.854 ± 0.364[a]	−0.944	0.373
Micro-BAG	0.876 ± 0.344[ab]	0.982 ± 0.238[ab]	−1.120	0.295
Nano-BAG	1.044 ± 0.436[ab]	1.159 ± 0.408[ab]	−2.511	0.036
Hybrid-BAG	0.941 ± 0.316[ab]	1.074 ± 0.191[ab]	−1.988	0.082
Test statistic‡	2.706	2.970		
P‡	0.044	0.031		

BAG, bioactive glass; H_i, indentation (nano)hardness; SD, standard deviation

[a,b] Different superscript letters within a column indicate statistically significant differences between groups (*P* < 0.05)

† Comparison between demineralization and pH cycle within each group (paired-samples *t* test; *t* value)

‡ Comparison among groups within each column (one-way ANOVA, *F* value; Duncan post hoc test)

Table 2 summarizes the modulus of elasticity values of the enamel for all groups. Within-group comparisons revealed no statistically significant differences between the post-demineralization and post-pH cycling stages (P > 0.05). No significant differences were found among the groups after demineralization (F = 2.051, P = 0.106) or after pH cycling (F = 2.521, P = 0.056).

Table 2
Modulus of elasticity values of enamel in each group after demineralization and after pH cycle

Group	E_i after demineralization (GPa), mean ± SD	E_i after pH cycle (GPa), mean ± SD	Test statistic†	*P*†
Negative control	62.767 ± 15.857	64.289 ± 15.670	−1.197	0.265
Control	45.167 ± 13.570	46.356 ± 9.670	−0.519	0.617
Micro-BAG	53.411 ± 17.230	58.467 ± 16.486	−1.437	0.189
Nano-BAG	54.067 ± 13.232	59.433 ± 16.181	−1.874	0.098
Hybrid-BAG	49.222 ± 6.127	51.089 ± 6.019	−1.387	0.203
Test statistic‡	2.051	2.521		
P‡	0.106	0.056		

BAG, bioactive glass; E_i, modulus of elasticity; SD, standard deviation

† Comparison between demineralization and pH cycle within each group (paired-samples *t* test; *t* value)

‡ Comparison among groups within each column (one-way ANOVA, *F* value)

The %SHR values for all groups are summarized in Table 3. The highest mean %SHR was observed in the Micro-BAG group (22.69 ± 42.32%), followed by the Hybrid-BAG (21.89 ± 30.50%), Control (18.24 ± 37.57%), Nano-BAG (15.40 ± 19.02%), and Negative control (6.80 ± 18.48%) groups, with no significant difference among groups (F = 0.383, P = 0.820).

Table 3
Percentage of surface hardness recovery (%SHR) in each group

Group	%SHR, mean ± SD
Negative control	6.798 ± 18.480
Control	18.242 ± 37.565
Micro-BAG	22.690 ± 42.321
Nano-BAG	15.398 ± 19.017
Hybrid-BAG	21.892 ± 30.495
Test statistic[†]	0.383
P[†]	0.820
BAG, bioactive glass; SD, standard deviation; SHR, surface hardness recovery	
[†] Comparison among groups (one-way ANOVA, *F* value)	

SEM–EDS analysis was performed on a single specimen per group, and no statistical comparison was performed; the results are therefore descriptive. SEM images of the sealant–enamel interface of the specimen analyzed in each group are shown in Fig. 2. In the Negative control group, which received no sealant, the enamel surface appeared rough and granular at 2,500× (Fig. 2a). In all sealed groups, a gap or crack was visible along the sealant–enamel interface (Fig. 2b–e, arrows). Qualitatively, the gap appeared narrowest in the Nano-BAG group (Fig. 2d), more prominent in the Micro-BAG and Hybrid-BAG groups (Fig. 2c, e), and relatively thickest in the Control group without BAG (Fig. 2b). These observations were qualitative, and the gap width was not measured.

The mean weight and atomic percentages of Ca and P are shown in Table 4. Both the weight and atomic percentages of Ca were highest in the Nano-BAG group, followed by the Micro-BAG, Hybrid-BAG, Control, and Negative control groups, respectively. The percentages of P were highest in the Control group, followed by the Micro-BAG and Hybrid-BAG groups, for both weight and atomic measurements. The lowest weight percentage of P was observed in the Nano-BAG group (16.28 ± 5.61 wt%), and the lowest atomic percentage in the Negative control group (12.97 ± 2.50 at%). The weight-based Ca/P ratios (Table 5) followed a descending order of Nano-BAG (3.10 ± 2.98), Hybrid-BAG (2.08 ± 0.08), Micro-BAG (2.03 ± 0.42), Control (1.39 ± 0.68), and Negative control (1.31 ± 0.57).

Table 4
Mean weight and atomic percentages of Ca and P in the enamel adjacent to the sealant base in each group

Group	Ca (wt%)	P (wt%)	Ca (at%)	P (at%)
Negative control	23.46 ± 12.14	17.85 ± 2.67	13.40 ± 7.42	12.97 ± 2.50
Control	32.57 ± 14.52	23.51 ± 3.12	20.23 ± 9.81	18.37 ± 3.00
Micro-BAG	42.75 ± 8.24	21.09 ± 0.77	27.34 ± 6.48	17.31 ± 1.00
Nano-BAG	50.44 ± 14.46	16.28 ± 5.61	33.92 ± 13.26	13.63 ± 4.68
Hybrid-BAG	42.27 ± 4.20	20.27 ± 1.48	26.44 ± 3.77	16.39 ± 1.88
Values are mean ± SD of five measurement points on a single specimen per group, obtained by SEM-EDS after pH cycling. No statistical comparison was performed.				
at%, atomic percentage; BAG, bioactive glass; Ca, calcium; P, phosphorus; SD, standard deviation; SEM-EDS, scanning electron microscopy with energy-dispersive X-ray spectroscopy; wt%, weight percentage				

Table 5
Weight-based Ca/P ratio in the enamel adjacent to the sealant base in each group

Group	Ca/P ratio, mean ± SD
Negative control	1.31 ± 0.57
Control	1.39 ± 0.68
Micro-BAG	2.03 ± 0.42
Nano-BAG	3.10 ± 2.98
Hybrid-BAG	2.08 ± 0.08
Values are mean ± SD of five measurement points on a single specimen per group, obtained by SEM-EDS after pH cycling. No statistical comparison was performed	
BAG, bioactive glass; Ca/P, calcium-to-phosphorus ratio; SD, standard deviation; SEM-EDS, scanning electron microscopy with energy-dispersive X-ray spectroscopy	

DISCUSSION

The null hypothesis that BAG particle size would not affect the remineralization of enamel adjacent to resin-based fissure sealants could not be rejected, as no significant differences were found among the sealant groups in nanohardness, modulus of elasticity, or %SHR; however, only the Nano-BAG group showed a significant within-group increase in nanohardness after pH cycling. The mean increases in nanohardness after pH cycling were of similar magnitude across the sealant groups (0.091–0.133 GPa), so the significance reached only in the Nano-BAG group should be interpreted cautiously.

The limited long-term ion release and recharge capacity of fluoride-releasing resin sealants has prompted the investigation of bioactive fillers such as BAG [15–17]. In the present study, incorporating 15 wt% nano-sized BAG into the resin sealant was associated with a significant within-group increase in enamel nanohardness after pH cycling. However, the sealant groups did not differ significantly from one another, so these findings are preliminary and do not establish an advantage of nano-sized over micro-sized BAG.

Beyond compositional modifications, particle downsizing has been proposed to optimize bioactivity without compromising the physical integrity of resin systems [28–30]. Yang et al. [7] reported that nano-sized BAG particles offer greater acid-neutralizing effects and bioactivity than their micro-sized counterparts. Regarding filler loading, Chen et al. [31] noted that while increasing filler content can enhance remineralizing capacity, exceeding a 20 wt% threshold may negatively affect mechanical performance. Khvostenko et al. [32] reported that resin matrices containing up to 15 wt% unsilanated BAG exhibit mechanical properties comparable or superior to commercial products, while Tauböck et al. [33] reported that 20 wt% BAG remains clinically acceptable regarding viscosity and degree of conversion. Specifically evaluating particle size, Odermatt et al. [29] showed that reducing 15 wt% BAG fillers to nano-dimensions does not adversely affect polymerization kinetics. The 15 wt% loading used in the present study is within the range reported to be compatible with the mechanical performance of resin matrices. However, mechanical properties, viscosity, and degree of conversion were not evaluated here, and our data do not allow conclusions on the structural integrity of the experimental sealants.

While previous research has extensively evaluated BAG incorporation into glass ionomer cements and composite resins [29, 32–35], studies focusing on BAG-modified fissure sealants remain comparatively limited [7, 8, 22]. In vitro evidence indicates that BAG-filled materials induce a localized increase in pH and promote the formation of Ca–P precipitates [7, 36, 37]. This apatite-forming potential has been proposed to help seal microgaps at tooth–restoration margins and reduce bacterial penetration [38]. In the present study, a gap or crack was visible along the sealant–enamel interface in all sealed groups on SEM. Although the gap appeared narrowest in the Nano-BAG group and thickest in the Control group, these qualitative observations were limited to a single specimen per group, the gap width was not measured, and some gaps may have been introduced during specimen preparation. Therefore, our findings neither confirm nor exclude a sealing effect of BAG at the interface.

Beyond particle size, the effectiveness of BAG-modified fissure sealants is thought to be linked to their acid-neutralizing capacity and ion release [7, 8]. The release of Ca^{2+}, PO_4^{3-}, and Na^{+} ions from BAG may buffer acidic microenvironments and resist demineralization [8, 22], and this pH-buffering action may promote a state of supersaturation with respect to hydroxyapatite at the tooth–sealant interface during cariogenic challenges. Such a mechanism could contribute to the significant within-group increase in nanohardness observed in the Nano-BAG group during the 7-day pH-cycling regimen. However, ion release, local pH, and surface reactivity were not measured, and the absence of significant differences among the sealant groups does not allow this finding to be attributed specifically to the nano-sized particles.

Previous studies have reported greater remineralization potential for nano-sized BAG than for micro-sized counterparts. Vollenweider et al. [39] reported enhanced remineralization efficacy with nanoscale bioactive glass particles, and Odermatt et al. [29] reported that reducing BAG filler dimensions promotes the precipitation of a more uniform hydroxyapatite layer. In the present study, mean enamel nanohardness increased in all groups following pH cycling, and this increase reached statistical significance only in the Nano-BAG group ($P = 0.036$). However, the mean increases were of similar magnitude across the sealant groups, the increase was numerically largest in the Hybrid-BAG group (0.133 GPa vs. 0.115 GPa in the Nano-BAG group), %SHR was highest in the Micro-BAG group, and no significant differences were found among the sealant groups. Descriptively, the sealed groups showed larger mean increases (0.091–0.133 GPa) than the unsealed Negative control (0.021 GPa), although this was not tested statistically. Our findings are therefore compatible with, but do not confirm, a role of particle size in remineralization.

To precisely evaluate these localized mechanical changes, nanoindentation was selected over conventional microhardness testing due to its superior spatial resolution and sensitivity. This technique enables the detection of subtle hardness alterations at the early stages of enamel demineralization and remineralization, while simultaneously calculating both nanohardness and elastic modulus from a single indentation depth curve [40]. Consequently, it provides a comprehensive, depth-resolved assessment of the mechanical properties of the superficial enamel adjacent to the sealant interface.

The technical utility of nanoindentation is well reflected in studies evaluating enamel micro-structural alterations. Huang et al. [41] reported baseline surface enamel nanohardness and elastic modulus ranges of 2.84–3.58 GPa and 54.8–65.9 GPa, respectively, noting a progressive decrease in mechanical properties with increasing substrate depth. Similarly, Zheng et al. [42] observed a nanohardness of 1.60 ± 0.20 GPa and an elastic modulus of 64.89 ± 5.50 GPa in citric acid-demineralized enamel. In the present study, post-demineralization nanohardness values (0.763–1.341 GPa) were lower than those reported for sound enamel [41] and for citric acid-demineralized enamel [42], and elastic modulus values (45.2–62.8 GPa) were similar to or lower than the reported ranges. This is consistent with demineralization, although sound enamel was not measured in this study, so the extent of demineralization could not be verified. High standard deviations in such measurements are frequently attributed to the heterogeneous micro-architecture of lesion substrates [43, 44], and the variability in our findings may also reflect differences in demineralization response among teeth and localized surface roughness. Notably, nanohardness differed among groups after demineralization, before any sealant had been applied ($P = 0.044$), indicating baseline differences that may have influenced comparisons of absolute values after pH cycling. Because each specimen served as its own control, within-specimen changes were not affected by differences in baseline hardness among teeth; however, enamel was not measured before demineralization, so these baseline differences could not be attributed to allocation or to differential lesion formation.

The relationship between enamel nanohardness and elastic modulus during mineral precipitation is intricate. Vollenweider et al. [39] observed that while bioactive glass promotes remineralization, the

resulting elastic modulus often remains comparable to demineralized substrates, likely due to the unorganized structural arrangement of newly deposited mineral phases. Similarly, Barbour et al. [40] highlighted that alterations in hardness and elastic modulus do not necessarily follow a linear or proportional rate, reflecting different structural determinants. In the present study, no statistically significant differences in elastic modulus were observed within groups between the two stages or among groups ($P > 0.05$). This may be attributed to the unorganized arrangement of newly deposited mineral, as described above, or simply to the absence of a measurable change in elastic modulus. The 7-day pH-cycling duration may also have been insufficient for the mineral maturation required to modify the elastic properties of the enamel.

The Ca/P ratio is a chemical indicator of enamel mineral composition, with stoichiometric hydroxyapatite classically exhibiting an atomic Ca/P ratio of 1.67 [45]. While demineralization depletes this ratio, exposure to bioactive remineralizing agents may restore or elevate localized calcium and phosphate concentrations [46], and previous investigations of BAG-based formulations have reported Ca/P ratios approaching or exceeding natural hydroxyapatite values [47–49]. In the present study, the weight-based Ca/P ratios were numerically higher in all BAG-containing groups than in the Control and Negative control groups, and the Nano-BAG group showed the highest Ca percentages and Ca/P ratio (Tables 4 and 5). Because the 1.67 reference applies to atomic ratios, the atomic Ca/P ratios calculated from the mean at% values (see Results) are more appropriate for this comparison: only the Nano-BAG group (2.49) exceeded the stoichiometric value, whereas the Micro-BAG (1.58) and Hybrid-BAG (1.61) groups remained below it. However, these findings should be interpreted with caution. EDS was performed on a single specimen per group without statistical comparison, and no EDS measurement was available from sound enamel or before sealant application, so the values cannot be attributed to remineralization. The Nano-BAG group also showed considerable variability among the five measurement points (Ca/P 3.10 ± 2.98), and its Ca content (50.44 wt%) exceeded that expected for hydroxyapatite (approximately 40 wt%), which may indicate a contribution of BAG particles or sealant filler within the analyzed volume. Descriptively, these results are consistent with a higher calcium content near BAG-containing sealants, but they do not demonstrate enamel remineralization.

When evaluating relative recovery through %SHR, no statistically significant differences were detected among the groups ($P = 0.820$). Although the Micro-BAG group exhibited the highest numerical mean %SHR (22.69 ± 42.32%), the data were characterized by notably high standard deviations in all groups. This variability may reflect the high spatial sensitivity of nanoindentation and the heterogeneous distribution of manually incorporated BAG fillers. It may also reflect the calculation itself: because %SHR is expressed relative to the post-demineralization hardness, groups with lower initial values (such as the Control group, 0.763 GPa) may show inflated relative recovery, and baseline differences among groups may have contributed to the dispersion.

The findings of this study should be interpreted within the context of several limitations. First, SEM–EDS was performed on a single specimen per group, and its five measurement points do not represent independent replicates, so no statistical comparison was possible. EDS measurements were also not

obtained from sound enamel or before sealant application, and the gaps observed at the sealant–enamel interface were not measured and may partly reflect specimen preparation. Second, enamel nanohardness was not measured before demineralization, and the groups differed in nanohardness after demineralization, which may have influenced comparisons of absolute values. Third, filler dispersion was achieved by manual mixing, which may have caused micro-scale heterogeneity, and ion release, local pH, degree of conversion, and mechanical properties such as shear bond strength and wear resistance were not evaluated. Finally, as an in vitro study on flat, polished enamel, this setup cannot replicate fissure morphology or the complex oral microenvironment, including salivary clearance, biofilm interactions, and thermal fluctuations, and the 7-day pH-cycling period may not capture long-term performance.

CONCLUSIONS

Within the limitations of this in vitro study, nano-BAG incorporation into a resin-based fissure sealant showed a significant within-group increase in enamel nanohardness after pH cycling, although the sealant groups did not differ significantly from one another. These preliminary findings support further investigation of nano-BAG–modified sealants, including larger samples, characterized fillers, and mechanical and ion-release testing.

Declarations

Ethics approval and consent to participate: The study protocol was approved by the Non-Interventional Clinical Research Ethics Committee of Bezmialem Vakıf University (Istanbul, Turkey) (approval no. 2021/128). All experiments were performed in accordance with relevant guidelines and regulations, including the Declaration of Helsinki. Written informed consent was obtained from all patients prior to tooth collection.

Consent for publication: Not applicable

Availability of data and materials: The datasets used and/or analysed during the current study are available from the corresponding author on reasonable request**.**

Competing interests: The authors declare that they have no competing interests

Funding: This study was supported by the Scientific Research Project Support of Bezmialem Vakıf University (Project No: 20210412).

Authors' contributions: PKT and GABC conceived the ideas, ACÖ, CE, and GABC collected the data, ACÖ and GABC analyzed the data, GABC and PKT led the writing, and SY was the supervisor. All authors read and approved the final manuscript.

Acknowledgements: Not applicable

References

1. Petersen PE. World Health Organization global policy for improvement of oral health—World Health Assembly 2007. Int Dent J. 2008;58(3):115–21.
2. Leal SC. Minimal intervention dentistry in the management of the paediatric patient. Br Dent J. 2014;216(11):623–7.
3. Fejerskov O. Changing paradigms in concepts on dental caries: consequences for oral health care. Caries Res. 2004;38(3):182–91.
4. Jurić H. Current possibilities in occlusal caries management. Acta Med Acad. 2013;42(2):216.
5. Goršeta K. Fissure sealing in occlusal caries prevention. Emerging Trends in Oral Health Sciences and Dentistry. IntechOpen; 2015.
6. Beauchamp J, Caufield PW, Crall JJ, Donly K, Feigal R, Gooch B, et al. Evidence-based clinical recommendations for the use of pit-and-fissure sealants. J Am Dent Assoc. 2008;139(3):257–68.
7. Yang SY, Piao YZ, Kim SM, Lee YK, Kim KN, Kim KM. Acid neutralizing, mechanical and physical properties of pit and fissure sealants containing 45S5 bioactive glass. Dent Mater. 2013;29(12):1228–35.
8. Yang SY, Kwon JS, Kim KN, Kim KM. Enamel surface with pit and fissure sealant containing 45S5 bioactive glass. J Dent Res. 2016;95(5):550–7.
9. Fei X, Li Y, Weir MD, Baras BH, Wang H, Wang S, Sun J, Melo MAS, Ruan J, Xu HHK. Novel pit and fissure sealant containing nano-CaF2 and DMAHDM. Dent Mater. 2020;36(9):1241–53.
10. Carlsson A, Petersson M, Twetman S. Clinical performance of a fluoride-containing fissure sealant. Am J Dent. 1997;10(3):115–9.
11. Hicks MJ, Flaitz CM, Garcia-Godoy F. Fluoride-releasing sealant and enamel lesion formation. J Clin Pediatr Dent. 2000;24(3):215–9.
12. Salar DV, Garcia-Godoy F, Flaitz CM, Hicks MJ. Inhibition of demineralization by fluoride-releasing sealants. J Am Dent Assoc. 2007;138(4):502–6.
13. Lobo MM, Pecharki GD, Tengan C, da Silva DD, Tagliaferro EPS, Napimoga MH. Fluoride-releasing capacity and cariostatic effect. J Oral Sci. 2005;47(1):35–41.
14. Prabhakar AR, Dahake PT, Raju OS, Basappa N. Fluoride in fissure sealants. Int J Clin Pediatr Dent. 2012;5(1):1–5.
15. Chole D, Lokhande P, Shashank K, Bakle S, Devagirkar A, Dhore P. Fluoride release and recharge of sealants. Int J Adv Health Sci. 2015;2:1–6.
16. Bayrak S, Tunc ES, Aksoy A, Ertas E, Guvenc D, Ozer S. Fluoride release and recharge from fissure sealants. Eur J Dent. 2010;4(3):245–50.
17. Heifetz SB, Yaari A, Proskin H. Anticaries effectiveness of sealants. J Calif Dent Assoc. 2007;35(8):573–7.

18. Imazato S. Antibacterial properties of resin composites and bonding systems. Dent Mater. 2003;19(6):449–57.
19. Jones JR. Review of bioactive glass: from Hench to hybrids. Acta Biomater. 2013;9(1):4457–86.
20. Skallevold HE, Rokaya D, Khurshid Z, Zafar MS. Bioactive glass applications in dentistry. Int J Mol Sci. 2019;20(23):5960.
21. de Oliveira AAR, de Souza DA, Dias LLS, de Carvalho SM, Mansur HS, Pereira MM. Bioactive glass nanoparticles. Biomed Mater. 2013;8(2):025011.
22. Lee MJ, Kim JY, Seo JY, Mangal U, Cha JY, Kwon JS, Choi SH. Resin-based sealant with bioactive glass. Nanomaterials. 2020;10(8):1581.
23. Özarslan AC, Yücel S. Strontium-incorporated bioactive glass scaffolds. Mater Sci Eng C. 2016;68:350–7.
24. Cacciotti I, Lombardi M, Bianco A, Ravaglioli A, Montanaro L. Sol–gel derived 45S5 bioglass. J Mater Sci Mater Med. 2012;23:1849–56.
25. Ten Cate JM. Chemical interactions between the tooth and oral fluids. In: Dental Caries: The Disease and Its Clinical Management. 2003.
26. Featherstone JDB. Enhancement of remineralization in vitro and in vivo. In: Factors Relating to Demineralisation and Remineralisation of Teeth. 1986.
27. Amaechi BT, Ramalingam K, Mensinkai PK, Chedjieu I. Remineralization by high-fluoride dentifrice. Gen Dent. 2012;60(4):e186–92.
28. Melo MAS, Guedes SFF, Xu HHK, Rodrigues LKA. Nanotechnology-based restorative materials. Trends Biotechnol. 2013;31(8):459–67.
29. Odermatt R, Mohn D, Wiedemeier DB, Attin T, Tauböck TT. Nano vs micro bioactive glass composites. J Clin Med. 2020;9(3):772.
30. Mitra SB, Wu D, Holmes BN. Nanotechnology in dental materials. J Am Dent Assoc. 2003;134(10):1382–90.
31. Chen L, Yu Q, Wang Y, Li H. Hydroxyapatite nanofiber composites. Dent Mater. 2011;27(11):1187–95.
32. Khvostenko D, Mitchell JC, Hilton TJ, Ferracane JL, Kruzic JJ. Bioactive glass composites. Dent Mater. 2013;29(11):1139–48.
33. Tauböck TT, Zehnder M, Schweizer T, Stark WJ, Attin T, Mohn D. Bioactive dentin bonding resin. Dent Mater. 2014;30(8):868–75.
34. Yli-Urpo H, Närhi T, Söderling E. Antimicrobial effects of bioactive glass. Acta Odontol Scand. 2003;61(4):241–6.
35. Hyun HK, Salehi S, Ferracane JL. Biofilm formation effects. Dent Mater. 2015;31(12):1599–608.
36. Yli-Urpo H, Närhi M, Närhi T. Tooth mineralization effects. Biomaterials. 2005;26(30):5934–41.
37. Yli-Urpo H, Vallittu PK, Närhi TO, Forsback AP, Väkiparta M. Ion release from bioactive glass. J Biomater Appl. 2004;19(1):5–20.

38. Khvostenko D, Hilton T, Ferracane J, Mitchell J, Kruzic J. Bacterial penetration reduction. Dent Mater. 2016;32(1):73–81.
39. Vollenweider M, Brunner TJ, Knecht S, Grass RN, Zehnder M, Imfeld T, Stark WJ. Remineralization using bioactive glass. Acta Biomater. 2007;3(6):936–43.
40. Barbour ME, Parker DM, Jandt KD. Enamel dissolution and saturation. J Colloid Interface Sci. 2003;265(1):9–14.
41. Huang T, He L, Darendeliler M, Swain M. Nano-indentation of white spot lesions. Caries Res. 2010;44(2):101–7.
42. Zheng L, Zheng J, Weng L, Qian L, Zhou Z. Remineralization and nanomechanical properties. Wear. 2011;271(9–10):2297–304.
43. Mahoney EK, Rohanizadeh R, Ismail F, Kilpatrick N, Swain M. Hypomineralised enamel properties. Biomaterials. 2004;25(20):5091–100.
44. Angker L, Nockolds C, Swain MV, Kilpatrick N. Mechanical properties of carious dentine. Arch Oral Biol. 2004;49(5):369–78.
45. Hicks J, Garcia-Godoy F, Flaitz C. Biological factors in dental caries. J Clin Pediatr Dent. 2005;28(2):119–24.
46. Hegde MN, Moany A. CPP-ACP remineralization study. J Conserv Dent. 2012;15(1):61.
47. Kim HJ, Mo SY, Kim DS. Bioactive glass varnish Mater. 2021;14(13):3745.
48. Abbassy MA, Bakry AS, Alshehri NI et al. Bioglass paste and enamel protection. J Orthod Sci 2019;8.
49. Bakry AS, Marghalani HY, Amin OA, Tagami J. Bioglass and enamel erosion. J Dent. 2014;42(11):1458–63.

Figures

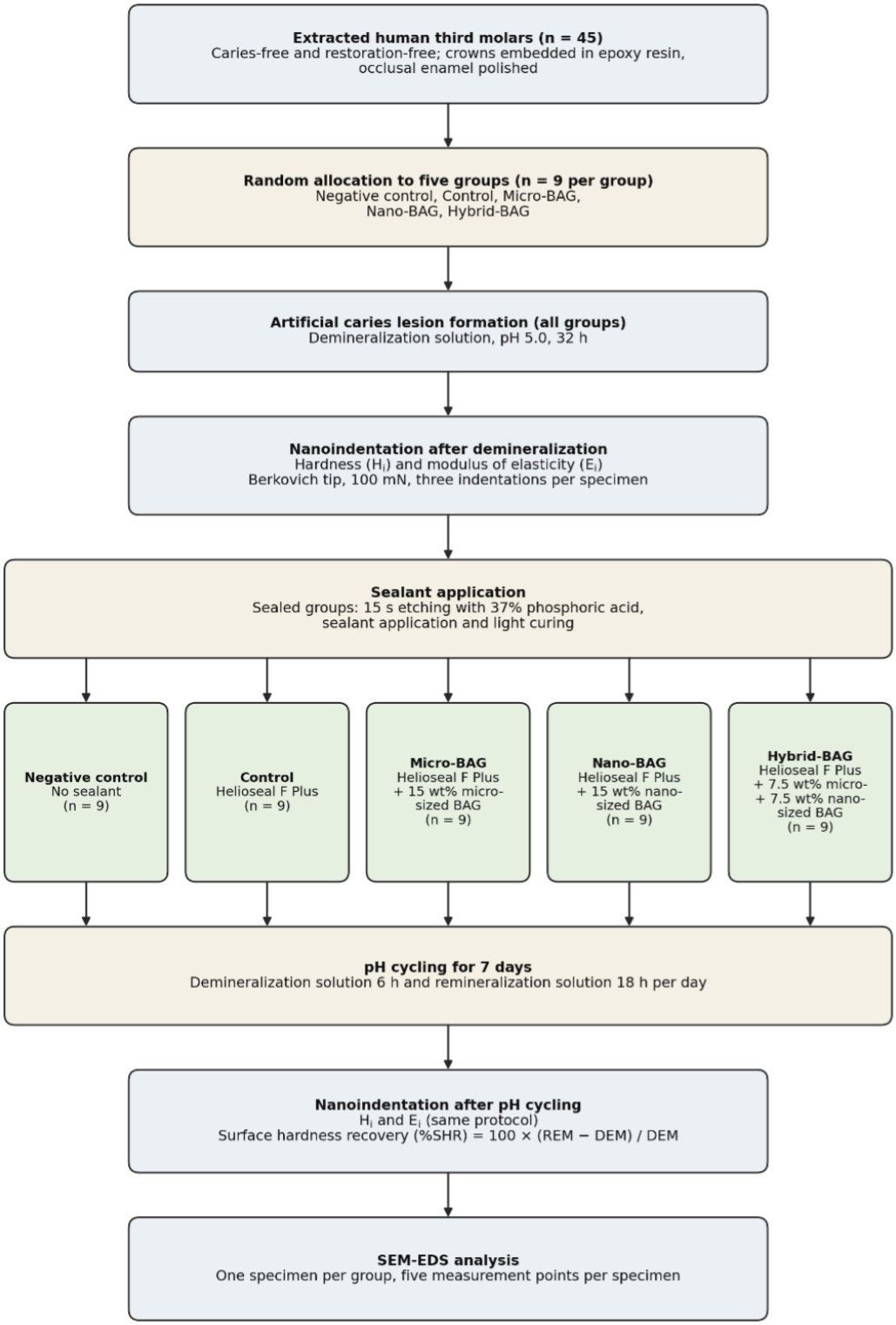


Figure 1

Study design. Human third molars (n = 45) were randomly allocated to five groups (n = 9 per group) and demineralized, and nanoindentation was performed. Sealants were then applied, and specimens were subjected to pH cycling and re-tested. SEM-EDS analysis was performed on one specimen per group. BAG, bioactive glass; DEM, hardness after demineralization; E_i, modulus of elasticity; H_i, nanohardness;

REM, hardness after pH cycling; SEM-EDS, scanning electron microscopy with energy-dispersive X-ray spectroscopy; %SHR, percentage of surface hardness recovery

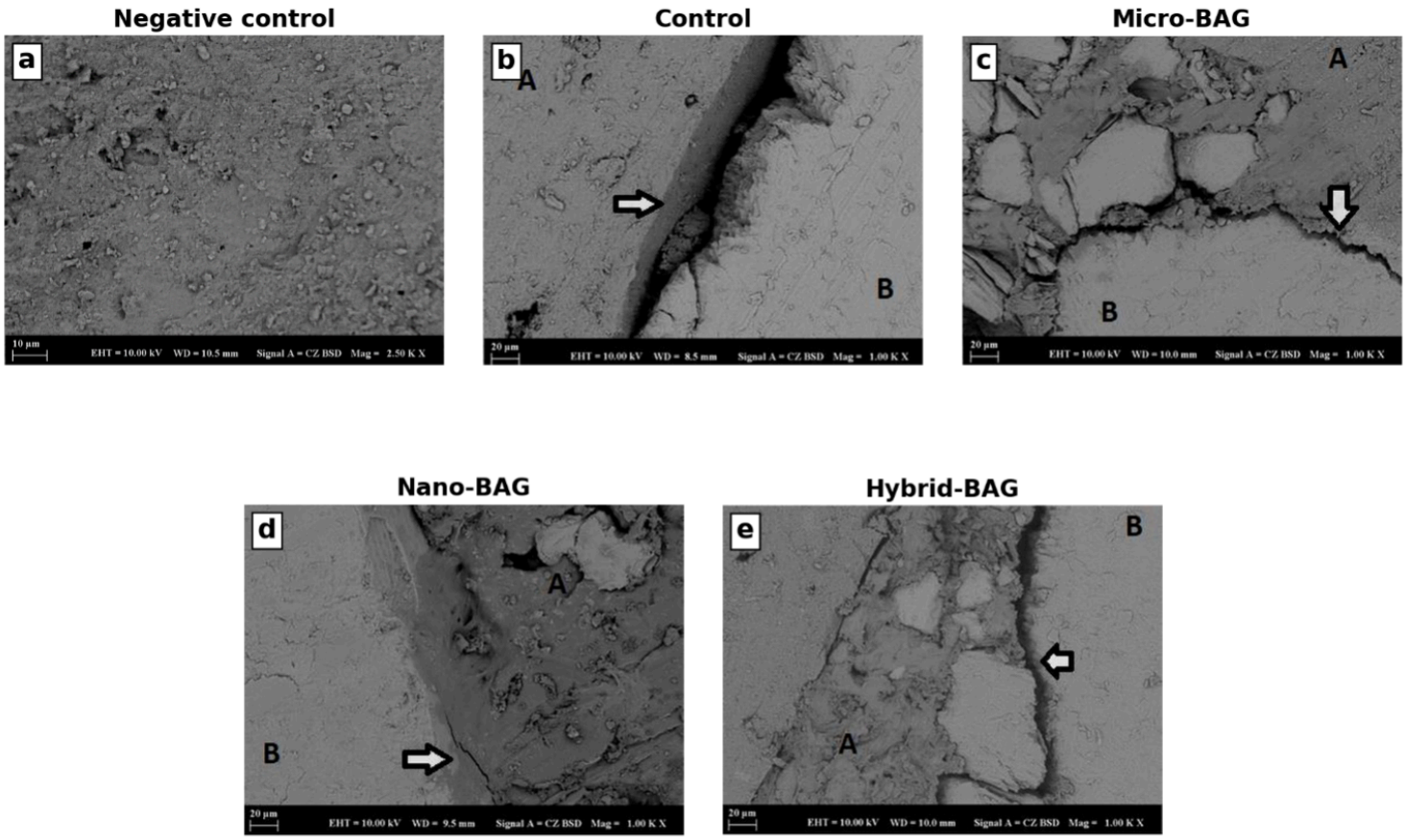


Figure 2

SEM images of the sealant–enamel interface of the single specimen analyzed in each group. (a) Negative control (no sealant, 2500×), (b) Control, (c) Micro-BAG, (d) Nano-BAG, (e) Hybrid-BAG (b–e, 1000×). A, fissure sealant; B, enamel; arrows, sealant–enamel interface. BAG, bioactive glass; SEM, scanning electron microscopy